UC Irvine

Title

Absolute band-edge energies are over-emphasized in the design of photoelectrochemical materials

Authors

Kaufman, Aaron J

Nielander, Adam C

Meyer, Gerald J

et al.

Absolute band-edge energies are over-emphasized in the design of photoelectrochemical materials

Aaron J. Kaufman ●[1], Adam C. Nielander ●[2], Gerald J. Meyer ●[3], Stephen Maldonado[4], Shane Ardo ●[5] & Shannon W. Boettcher ●[1,6,7] ✉

The absolute band-edge potentials of semiconductors and their positions relative to solution redox potentials are often invoked as design principles for photoelectrochemical devices and particulate photocatalysts. Here we show that these criteria are not necessary and limit the exploration of materials that may advance the fields of photoelectrochemistry, photochemistry and photocatalysis. We discuss how band-edge energies are not singular parameters and instead shift with pH, electrolyte type and surface chemistry. The free energies of electrons and holes, rather than those of solution redox couples, dictate overall reaction spontaneity and thus reactivity. Favourable charge-transfer kinetics can occur even when the relevant electrolyte redox potential(s) appear outside the bandgap, enabled by the inversion or accumulation of electronic charge at the semiconductor surface. This discussion informs design principles for photocatalytic systems engineering for both one-electron and multi-electron redox reactions (for example, H_2 evolution, H_2O oxidation and CO_2 reduction).

Suppose one desires to identify a semiconductor material that can photoreduce a species with a formal reduction potential $\varepsilon^{o'}$. Such a reduction could be a one-electron transfer for application in organic synthesis, environmental remediation or solar energy conversion, or a kinetically complex multi-electron transfer as in the reduction of H_2O or H^+ to H_2 fuel. A typical starting point would be to consult a photoelectrochemistry review article for the band-edge positions of semiconducting materials relative to the vacuum energy level and/or standard hydrogen electrode energy level, typically in an aqueous electrolyte[1–4]. With the knowledge that bandgap photoexcitation creates electron–hole pairs that relax/thermalize to the band edges before interfacial electron transfer occurs, an inspection of the tabulated conduction-band-edge energy (E_c) relative to $-q\varepsilon^{o'}$ would allow one to

predict whether a given semiconductor was appropriate for the desired reaction (the variables used in this contribution are defined in Table 1). One might also conclude that interfacial electron transfer from the semiconductor into solution would not occur at all if $-q\varepsilon^{o'} > E_c$, that is, if the reduction potential lies above the conduction-band energy. These ideas are misleading and are often not the limiting property for photoelectrochemical devices and particulate photocatalysts. Distinct rate processes developing excess charge, described in this Perspective, can move the tabulated E_c value relative to the $-q\varepsilon^{o'}$ without a chemical transformation. A reduction potential that falls outside the semiconductor bandgap may impact the current–voltage behaviour and voltage-dependent interfacial kinetics, but does not in fact preclude facile electron transfer.

[1]Department of Chemistry and the Oregon Center for Electrochemistry, University of Oregon, Eugene, OR, USA. [2]SUNCAT Center for Interface Science and Catalysis, SLAC National Accelerator Laboratory, Menlo Park, CA, USA. [3]Department of Chemistry, University of North Carolina at Chapel Hill, Chapel Hill, NC, USA. [4]Department of Chemistry and Program in Applied Physics, University of Michigan, Ann Arbor, MI, USA. [5]Department of Chemistry, Department of Chemical and Biomolecular Engineering and Department of Materials Science and Engineering, University of California, Irvine, CA, USA. [6]Department of Chemical and Biomolecular Engineering and Department of Chemistry, University of California, Berkeley, CA, USA. [7]Energy Storage and Distributed Resources Division, Lawrence Berkeley National Laboratory, Berkeley, CA, USA. ✉e-mail: boettcher@berkeley.edu

Table 1 | Definitions of the variables used in this Perspective

Term	Symbol	Unit	Brief definition
Elementary charge	q	C	Magnitude of charge on a single electron (F/N_A)
Stoichiometric number	v_i	Unitless	Number of species i in a balanced equation
Signed charge number	z_i	Unitless	Signed charge number of species i (for example, +2, +1, 0, −1, −2)
Avogadro's constant	N_A	mol^{-1}	Number of entities in 1 mol of a given substance
Faraday constant	F	C mol^{-1}	Magnitude of charge per mole of protons
Electron-transfer rate constant	$k_{rxn,et}$, $k'_{rxn,et}$	cm^4 s^{-1}	Electron-transfer (et) rate constant for a second-order heterogeneous surface reaction; the prime indicates the reverse reaction
Hole-transfer rate constant	$k_{rxn,ht}$, $k'_{rxn,ht}$	cm^4 s^{-1}	Hole-transfer (ht) rate constant for a second-order heterogeneous surface reaction; the prime indicates the reverse reaction
Electron concentration	n, $n_{rxn,s}$, $n^{eq}_{rxn,s}$	cm^{-3}	Concentration of electrons in the conduction band (n), the surface concentration is denoted by subscript s and eq indicates the equilibrium value
Hole concentration	p, $p_{rxn,s}$, $p^{eq}_{rxn,s}$	cm^{-3}	Concentration of holes in the valence band (p), the surface concentration is denoted by subscript s and eq indicates the equilibrium value
Activity	a_i^α	Unitless	The activity of species i in phase α is defined by $a_i^\alpha = \gamma_i^\alpha C_i^\alpha / C_i^{0,\alpha}$, where, γ_i^α is the activity coefficient, C_i^α is the concentration and $C_i^{0,\alpha}$ is a reference concentration, usually taken to be 1 M for soluble species
Electrostatic potential	ϕ	V	Electrical work needed to move a test charge to a specific point in space from a reference point (often at infinite distance) divided by the value of the charge
Reduction potential	ε	V	Free-energy change divided by the electron charge associated with moving an electron (and any associated ion/solvent movement/rearrangement) from a reference state (often a reference electrode) into the bulk of a solution via a redox reaction
Formal reduction potential	$\varepsilon^{o\prime}$	V	Potential measured for a reduction reaction with a standard-state concentration for each species
Effective conduction and valence band density of states	N_C and N_V	cm^{-3}	The number per volume of thermally accessible electron and hole states at E_c and E_v, respectively
Charge density	ρ	C cm^{-3}	The amount of electric charge per unit volume
Debye length	λ	cm	A characteristic length over which mobile charge carriers screen an electric field, which decreases with mobile carrier density
Depletion width	w	cm	Length over which mobile carriers are depleted at a doped semiconductor surface or junction
Donor and acceptor density	N_D and N_A	cm^{-3}	Number density of electrons and holes donated to the conduction and valence band, respectively, by impurity atoms
Vacuum energy level	E_{vac}	eV	Energy of a free stationary electron outside of a material, typically defined to be zero
Conduction and valence band edge	E_c and E_v	eV	Energies analogous to the LUMO and HOMO for semiconductor solids (often referenced to the vacuum energy level)
Bandgap	E_g	eV	Energy separation between E_c and E_v
Electrochemical potential	$\bar{\mu}_i^\alpha$	J mol^{-1}	Partial molar Gibbs free energy of a given species i in phase α, which defines the criteria for equilibrium
Chemical potential	μ_i^α	J mol^{-1}	Partial molar Gibbs free energy, ignoring long-range electrostatic contributions
Fermi level	E_f, E_{fp}, E_{fn}	eV	Electrochemical potential ($\bar{\mu}_e^\alpha$) of electrons in phase α; the subscripts p and n denote carriers only in the valence or conduction band, respectively
Gibbs free energy	G	J	Thermodynamic potential used to calculate the maximum amount of non-pressure-volume work that may be performed at constant temperature and pressure
Open-circuit voltage	V_{oc}	V	The difference in the electron electrochemical potential (divided by charge) between two contacts with no external current flow
Partial current density	$J_n(x)$, $J_p(x)$	C s^{-1} cm^{-2}	The amount of electrical charge passed by electrons (n) or holes (p) per unit time per unit area at position x, which sum to the total charge density
Equilibrium exchange current density	J_{0n}^x, J_{0p}^x	C s^{-1} cm^{-2}	The partial current density at position x for electrons (n) or holes (p) at equilibrium
Temperature	T	K	Absolute temperature
Pressure	P	Pa	Force exerted per unit area
Ideal gas constant	R	J K^{-1} mol^{-1}	Avogadro's number multiplied by the Boltzmann constant
Differential capacitance	C_{sem}, C_{edl}	F cm^{-2}	Differential capacitance of the semiconductor, differential capacitance of the electrical double layer
Number of species in a phase	N_i	Number	The number of particles of the species i.

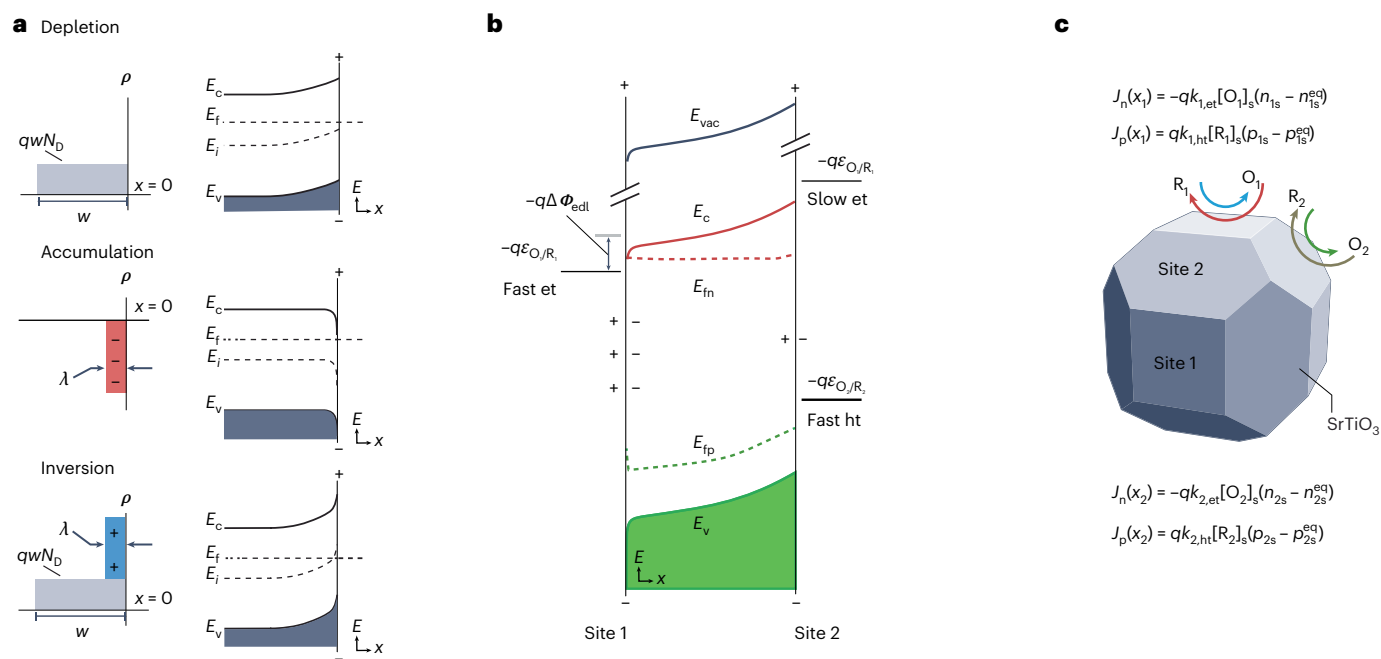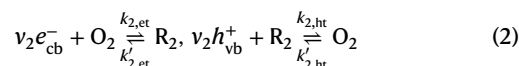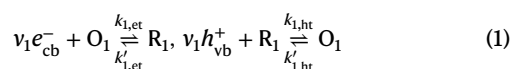rxn, reaction number; LUMO, lowest-unoccupied molecular orbital; HOMO, highest-occupied molecular orbital.

Fig. 1 | Interface energies and reactions. a, Excess charge-carrier-density plots (left) and band diagrams (right) for an n-type semiconductor in depletion, accumulation and inversion due to equilibration with a contacting phase (for example, redox species). **b**, Depleted photoabsorber particle (site 2) driving misaligned half reactions under illumination (simulated one-dimensional COMSOL Multiphysics model, $N_D = 10^{14}\ cm^{-3}$, length = 1 μm, and disparate electron-transfer (et) and hole-transfer (ht) rates at the electron- and hole-selective contacts, respectively). Accumulated surface electrons (site 1) pull up the photoabsorber energy levels relative to $q\varepsilon_{O_1/R_1}$ by an electrostatic potential energy $q\Delta\phi_{edl}$, allowing photoexcited electrons to drive a reduction reaction on the semiconductor surface whose energy is out of the bandgap. **c**, Possible facet-dependent oxidation and reduction kinetics and rate equations quantifying charge-carrier selectivity, as discussed in the text.

Tabulated band-edge positions are poor indicators of interfacial redox chemistry because they are not singular parameters—they are sensitive to the chemical environment and surface chemistry and are modulated by interface electrostatics. The free energies of non-equilibrium electronic charge carriers (for example, the hole and electron quasi-Fermi levels) in a semiconductor, at steady state and under illumination, determine their ability to drive overall reactions and perform chemical work[5]. The degree to which the quasi-Fermi levels split under illumination, in turn, depends on the kinetics of charge transfer; that is, the surfaces or interfaces acting as charge-carrier-selective contacts, not on the absolute band-edge energies. In this Perspective, we discuss the origins of the common misconception that absolute band edges are critical and illustrate the underlying design principles for improved materials and interfaces, operative charge-separation/collection mechanisms and stabilization strategies at semiconductor/electrolyte interfaces.

Governing equations

The purpose of this section is to show how the band-edge positions are not the critical parameters for the selection of semiconductors because they shift in response to carrier accumulation and surface chemistry. Consider a semiconductor without dopants and without interfacial electric fields at equilibrium (that is, the so-called flat-band condition). With generality to molecular, particulate and bulk semiconductor photoabsorbers, we can write the following equilibrium expressions for a pair of redox reactions (either outer-sphere one-electron reactions or multi-step electron-transfer reactions) that include both electrons (e_{cb}^-), holes (h_{vb}^+), and O (oxidized) and R (reduced) species, with the specific charge not included for simplicity of notation:

$$\nu_1 e_{cb}^- + O_1 \underset{k'_{1,et}}{\overset{k_{1,et}}{\rightleftharpoons}} R_1,\ \nu_1 h_{vb}^+ + R_1 \underset{k'_{1,ht}}{\overset{k_{1,ht}}{\rightleftharpoons}} O_1 \qquad (1)$$

$$\nu_2 e_{cb}^- + O_2 \underset{k'_{2,et}}{\overset{k_{2,et}}{\rightleftharpoons}} R_2,\ \nu_2 h_{vb}^+ + R_2 \underset{k'_{2,ht}}{\overset{k_{2,ht}}{\rightleftharpoons}} O_2 \qquad (2)$$

Marcus theory shows how the standard electron-transfer rate constant for an outer-sphere redox reaction (that is, where electron transfer is across the double layer) can be expressed in terms of the energy difference between the band edge and redox energy[6,7]. While in some (ideal) cases Marcus theory describes the kinetics of electron transfer from a semiconductor to molecular acceptors[8,9], photochemical fuel-forming reactions do not generally proceed as purely outer-sphere reactions, but instead involve catalytic species and mechanistic steps with inner-sphere intermediates (that is, species that may interact in the strong-coupling limit)[10]. Furthermore, band-edge positions are generally unknown under the experimental conditions of interest as they are not singular parameters. Ab initio calculations can provide a guide, but are limited in that they assume an atomic-scale structure and termination of the active surface and interface solvent/double-layer structure that is typically experimentally unknown. Predicting rate constants for practically relevant photoelectrochemical processes thus remains a major challenge.

The free energy of charge carriers in a semiconductor is described by their electrochemical potential ($\bar{\mu}_i^\alpha$). In general, assuming thermal equilibrium, for species i in phase α:

$$\bar{\mu}_i^\alpha = \mu_i^\alpha + z_i F\phi^\alpha = \left(\mu_i^{0\alpha} + RT\ln a_i^\alpha\right) + z_i F\phi^\alpha = N_a\left(\frac{\partial G}{\partial N_i}\right)_{T,P,N_{j\neq i}} \qquad (3)$$

Under illumination, one can separate the electrochemical potential of conduction band electrons from valence band holes. In semiconductor physics, these quantities are termed the electron and hole quasi-Fermi levels (E_{fn} and E_{fp}, respectively). Although quasi-Fermi
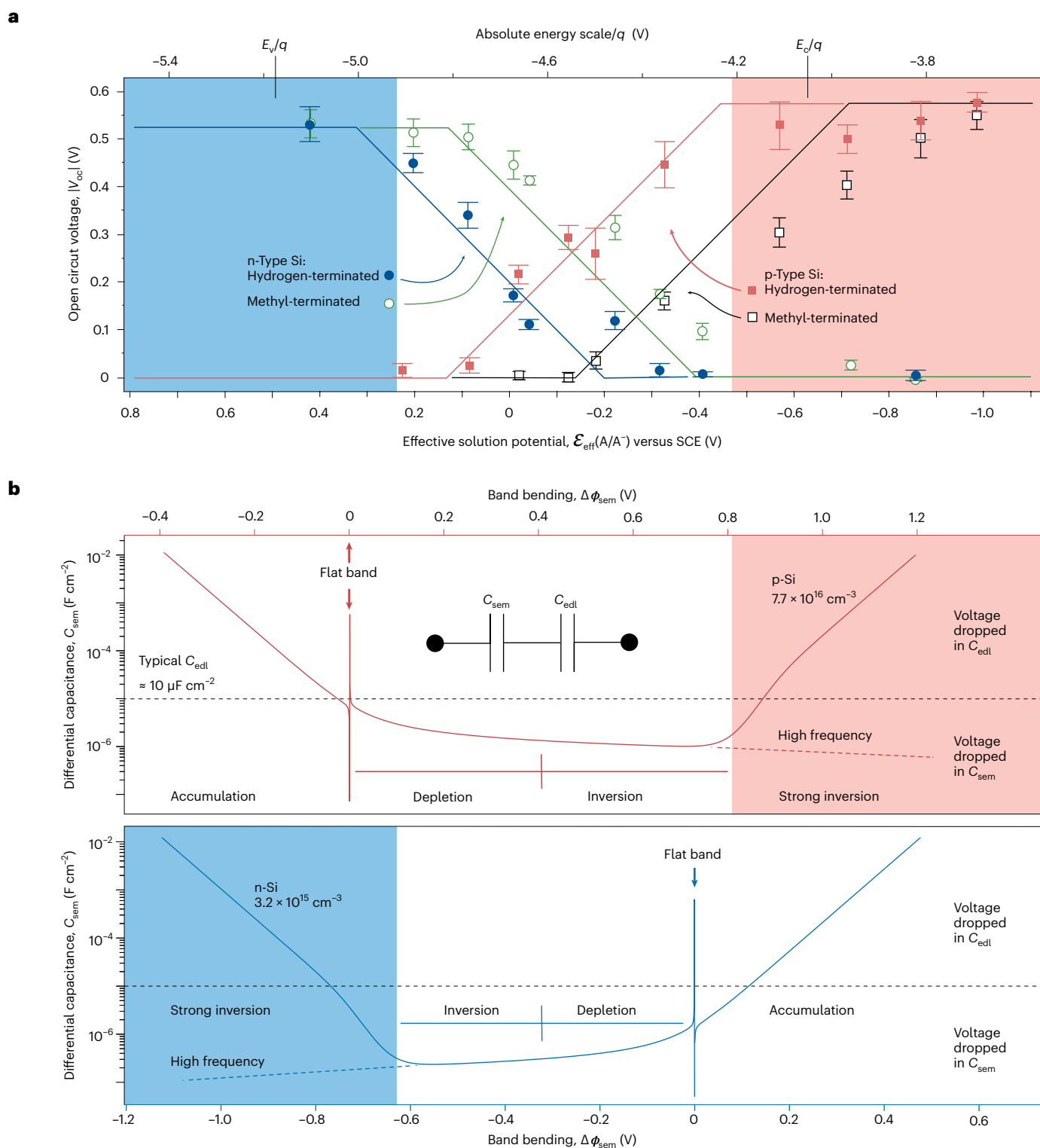
a

b

Fig. 2 | Accumulation, depletion and inversion at photochemical junctions.
a, The absolute value of V_{oc} ($|V_{oc}|$) measured for n- and p-type H- and CH$_3$-terminated Si with corresponding error bars as a function of the reducing power of the A/A$^-$ redox couple in the electrolyte, (ε_{eff}(A/A$^-$); data from ref. 22) that is aligned with the absolute energy scale and the differential capacitances in **b**. The solid lines are a guide to the eye and show the trends. Here, V_{oc} was directly measured from the semiconductor against a Pt electrode poised at the Nernstian potential of the solution (ε(A/A$^-$)) and plotted against the effective solution potential (ε_{eff}(A/A$^-$)), normalizing the minority-carrier acceptor concentration to 10 mM. The regions highlighted in blue and red correspond to strong inversion

for n-type Si (dopant density of 3×10^{15} cm^{-3}) and p-type Si (dopant density of 8×10^{16} cm^{-3}), respectively. **b**, Semiconductor differential capacitance (C_{sem}) for p-type Si (top) and n-type Si (bottom) at 295 K, taken from the calculated space-charge density[26], as a function of band bending ($\Delta\phi_{sem}$). The vertical asymptotes correspond to flat-band potentials. C_{sem} values have been plotted using the same dopant density as used by Grimm et al.[22] A double-layer capacitance (C_{edl}) of 10 μF cm^{-2} is shown as an approximate reference for relative voltage drops ($\Delta\phi_{edl}$ and $\Delta\phi_{sem}$). The expected high-frequency dark response in the inversion region is shown by a dashed line when the rate of generation of the minority carrier at the surface is low.

levels are understood for populations of electronic charge carriers, the concept applies in the ergodic limit to individual species[11]. For example, if a semiconductor particle is sufficiently small so that there are few excited carriers, the time-averaged behaviour is equivalent to the ensemble average across many particles, and energies can be described in terms of the quasi-Fermi level. Regardless of the band-edge position under the flat-band condition, the quasi-electrochemical potentials of conduction-band electrons and valence-band holes in the photoabsorber ($\bar{\mu}_n^{absr}$ and $\bar{\mu}_p^{absr}$, respectively) will tend towards equilibrium, transferring charge according to equations (1) and (2), or via the recombination of electrons and holes at the surface and within the bulk of the photoabsorber. To drive an overall uphill ($\Delta G_{rxn} > 0$) chemical reaction with light, the quasi-Fermi-level splitting ($E_{fn} - E_{fp}$) must be greater in magnitude than ΔG_{rxn} under steady-state reaction conditions (and relevant species activities at the surface). Differences between E_{fn} and E_{fp} beyond this minimum energy value are needed due to associated kinetic (catalytic) and mass-transport energy losses.

Semiconductor/liquid junctions

Next consider a wide-bandgap ($E_g \approx 3$–4 eV) semiconductor particle with a conduction band energy (or equivalently potential, which is the energy per charge on the relevant reference scale) that is not high enough to drive the hydrogen evolution reaction (that is, not reducing enough to drive the reduction of H_2O or H^+ to form H_2) but a valence band energy that is substantially below (that is, more oxidizing) the reversible oxygen reduction potential (Fig. 1). Under illumination, a small photoexcited carrier concentration (n' and p') is needed to produce the minimum thermodynamically required difference between $\bar{\mu}_n^{absr}$ and $-\bar{\mu}_p^{absr}$ to drive water splitting because of the low equilibrium concentrations of holes and electrons (n^{eq} and p^{eq}) in a wide-bandgap semiconductor. The total free energy available to drive chemical reactions is given by the difference between the electron and hole quasi-Fermi levels (or equivalent electrochemical potentials) according to equation (4).

$$\frac{F}{q}(E_{fn} - E_{fp}) = \frac{F}{q}E_g + RT \ln\frac{n'p'}{N_C N_V} = RT \ln\frac{n'p'}{n_i^2} > \Delta G_{rxn} (+ \Delta G_{losses})$$

(4)

where n_i is the intrinsic carrier concentration ΔG_{rxn} and ΔG_{losses} are the molar free energy of the reaction and that lost to the environment leading to inefficiency. Note that equation (4) does not include variables associated with the kinetics of the electron-transfer reactions or the absolute band-edge positions.

How can both electrons and holes transfer if the conduction-band-edge energy is not high enough to drive the reaction? Consider the following qualitative picture. The kinetics of hole transfer from semiconductor to solution species initially will be fast as the valence band holes are quite oxidizing, while electrons transfer slowly. This will lead to a build-up of negative electron charge on/in the semiconductor, which is equivalent to an applied negative bias that raises the electron quasi-Fermi level and eventually the band edges, increasing the reducing power of the photoexcited electrons. This process will occur until the rates of both hole and electron transfer are equal (at steady state). If the semiconductor particle is already doped n-type, as most metal oxides used in water splitting are[12–15], this negative charging under photoexcitation is termed majority carrier accumulation (electrons in an n-type semiconductor). The same phenomena can occur with the addition of excess minority carriers (holes in an n-type semiconductor), which is called inversion. The excess mobile carriers reside close to the surface of the semiconductor, typically within the first few atomic layers, as required by Gauss's law (Fig. 1a). This analysis assumes that there is no chemical change (for example, cation intercalation/deintercalation, changing surface termination or surface oxidation) that modifies the surface electrochemical potential without requiring the

development of excess space charge—such processes can also play an important role in dictating interfacial energetics[16–18].

Experimental data support the qualitative picture outlined above[19–22]. Grimm et al. showed systematic control of the interface photovoltage in H- and CH_3-terminated crystalline p-Si and n-Si photoelectrodes, governed by the reversible potential of the solution redox couple (Fig. 2a)[22]. These surfaces have low defect densities, with nearly every Si surface atom chemically terminated. If the redox potential of the solution was outside the bandgap of Si (that is, under flat-band conditions), the interface was driven into either inversion, where the minority carrier concentration at the surface exceeds that of the majority carriers in the semiconductor bulk, or accumulation, where excess majority carriers are at the surface[23]. Inversion creates the functional equivalent of a buried junction, leading to high photovoltages, while accumulation leads to an Ohmic contact between the solution and semiconductor.

While the regenerative photoelectrochemical cell architecture used by Grimm et al. has only one electrochemically active semiconductor interface, the demonstration of large (bulk-recombination-limited) photovoltages with solution potentials outside the absolute-energy limits of the Si bandgap is conceptually the same as the picture for the hypothetical wide-bandgap semiconductor described above. For example, the difference between the H- and CH_3-terminated surfaces leads to a systematic shift in the band-edge positions of ~0.4 V due to changes in the interface dipole. Regardless, there is no change in the maximum interface photovoltage or the ability to drive any given redox reaction irrespective of the reaction's redox potential[24]. The relative positions of the solution reduction potential/energy and the band edge energy positions do not determine the photochemical reactions that photoexcited carriers can drive. In fact, the highest photovoltages were observed for a p-Si photoelectrode in contact with a redox couple, dimethylcobaltocene (Fig. 2a), whose reduction potential close to −1 V versus the saturated calomel electrode (SCE) is much more negative than the conduction band edge (at flat band) for Si at about −0.6 V versus SCE[25,26]. The absolute conduction band energy/potential value is irrelevant for determining which reductions p-Si can drive due to, in this case, carrier inversion. Evidence for inversion has been reported at photoelectrochemical interfaces via near-surface channel conductance measurements[27], photocapacitance[28] and infrared spectroscopy[29].

In the absence of other observations, the data in Fig. 2a could also be explained by densities of surface states that prevent larger degrees of band bending and high photovoltages (that is, surface-state-induced Fermi-level pinning)[30,31]. However, near-surface channel conductance measurements on some of the systems are inconsistent with this possibility[27]. Nevertheless, when large densities of surface states do cause Fermi-level pinning, the resultant photoelectrode behaviour is like that of a buried junction or a photoelectrode in inversion—the photovoltage is independent of the redox potential of the solution and the absolute band-edge energies remain irrelevant with respect to which reactions can be driven.

The data in Fig. 2a come from measurements of the semiconductor operating under accumulation, depletion, or inversion conditions, which can be understood with equivalent-circuit models. At semiconductor/liquid junctions, the simplest model consists of two capacitors, one representing the charge stored in the semiconductor space charge region (C_{sem}) and the other the Helmholtz double layer (C_{edl}). More complex models that include a diffuse layer, interfacial surface states and other corrections can also be used[3], but they are not needed to illustrate accumulation, depletion and inversion conditions. The absolute electrostatic potential drops across the space charge region ($\Delta\phi_{sem}$) and double layer ($\Delta\phi_{edl}$) are inversely related to their relative capacitances by the conservation of charge (equation (5)), where equilibration of the surface electrochemical potential sets the degree of band bending and therefore the potential dropped in the semiconductor ($\Delta\phi_{sem}$; Fig. 2b).

$$\frac{\Delta\phi_{sem}}{\Delta\phi_{edl}} = \frac{C_{edl}}{C_{sem}} \qquad (5)$$

The surface charge and C_{sem} depend on the applied potential in a manner that can be calculated from carrier statistics and Poisson's equation[26], but the key point is that the magnitudes of the potential drops in each region depend on both C_{sem} and C_{edl}. The value of $\Delta\phi$ is thus larger across the region with the smaller capacitance between C_{sem} and C_{edl}. Simply, the smaller capacitance reflects where the electrostatic potential change is larger. Plots of measured capacitance as a function of electrode potential may thus illustrate when accumulation or depletion conditions are operative, but such data are rarely reported, presumably due to the presence of surface states[32].

As a semiconductor electrode is biased into accumulation, the experimentally measured capacitance (C_{exp}) increases and saturates to the value of C_{edl}. In this condition, $\Delta\phi_{edl}$ is larger than $\Delta\phi_{sem}$. That is, applying a bias to a semiconductor electrode in accumulation does not substantially move the (quasi-)Fermi levels relative to the band edges. Instead, the applied bias primarily shifts the band edges relative to a reference point in solution. Through equation (5), the quantity of charge from majority carriers (that is, $\Delta\phi_{sem} \times C_{sem}$) accumulated at the semiconductor surface must be counterbalanced exactly by the charge from ions in solution (that is, $\Delta\phi_{edl} \times C_{edl}$) gathered at the interface. Physically, the availability of ions from solution at this location is limiting because the abundance of majority carriers from within the semiconductor at the surface is large in accumulation, that is, C_{exp} tends to C_{edl}.

In depletion, the opposite is true. C_{exp} tends to C_{sem} because the total charge from the majority carriers in the semiconductor space charge region is much smaller than from the available ions in solution that could move to the interface. Correspondingly, $\Delta\phi_{sem}$ is substantially larger than $\Delta\phi_{edl}$ in depletion. This statement is equivalent to stating that the applied bias moves the (quasi-)Fermi levels relative to a reference point in solution, but the band-edge values are largely unchanged relative to that same reference point.

In accumulation, the interpretation of $\Delta\phi_{sem}$ is straightforward. C_{sem} is effectively independent of time/frequency because the equilibration of majority carriers from the bulk to the interface is fast on the relevant timescale of the impedance measurement. In inversion, the interpretation of $\Delta\phi_{sem}$ is more nuanced. C_{sem} can have a measurable time dependence as the supply of minority carriers to the surface depends on an interplay between the rate of thermal generation, drift, losses from recombination and consumption from interfacial processes. Accordingly, the measured capacitance–potential profile in inversion is a function of the frequency of measurement/observation (Fig. 2b, dashed versus solid line) and is strongly influenced by the operative kinetics of minority-carrier generation, transport, trapping and transfer[33]. This is why Mott–Schottky plots of impedance often remain linear in inversion at potentials well past the band edge and can make the increase in measured capacitance due to inversion difficult to observe[32,34–40].

Nanoscopic and molecular systems

In a bulk semiconductor, the number of band-edge states is large compared with the number of carriers at the surface. Thus, the chemical potential at the surface does not change with the build-up of charge (that is, the activity term a_i^α for charge carriers in equation (3) becomes nearly constant and is unaffected by further changes in carrier density at the surface, as in a polarized metal electrode).

Nanoscopic and molecular systems show similar behaviour (Fig. 3), but there are differences. Semiconductor nanoparticles are typically (practically) undoped, that is, their size limits the number of atomic substitutions. Yet, under illumination, they can accumulate electrons or holes at steady state. In general, the rates of photochemical electron and hole transfer are not initially identical following illumination. When the system reaches steady state, by definition, the time derivatives of all concentrations are zero. This means that the concentrations of electrons and holes build up to different extents such that it is the rates of photochemical electron and hole transfer that are ultimately balanced. This process leads to a steady-state electrostatic potential developing across the nanoparticle/solution interface. This change in $\Delta\phi$ moves the energies of the band edges relative to the solution reduction potential (or energy) for the reasons stated above. The steady-state electron and hole concentrations are thus defined by the reactant and product concentrations, charge-transfer rate constants and relevant generation/recombination mechanisms and rates.

For soluble molecular systems (M), the initial rates of electron and hole transfer will also not be identical in the ensemble of individual molecules. Molecular systems can thus also accumulate M$^-$ or M$^+$ at steady state (representing an additional negative or positive charge on M, which may also be initially charged). This process shifts the Nernst potential of the redox solution containing the ensemble of molecules through a change in the activities:

$$\varepsilon_{M^+/M} = \varepsilon^\circ_{M^+/M} + \frac{RT}{v_{e^-}F}\ln\frac{a_{M^+}}{a_M} \qquad (6)$$

and

$$\varepsilon_{M/M^-} = \varepsilon^\circ_{M/M^-} + \frac{RT}{v_{e^-}F}\ln\frac{a_M}{a_{M^-}} \qquad (7)$$

We note that this is different from a semiconductor particle that can build up charge at one energy level (the band edge) as electronic states are closely packed in energy. In a molecule, the electronic states are usually widely spaced in energy and thus this is not generally possible. Hence, there is no mechanism to smoothly vary the electric potential term for molecular systems via a process analogous to accumulation or inversion in a semiconductor. Instead, changes in chemical potential dominate contributions to changes in free energy under photoexcitation. As such, the primary mechanism to change the oxidation or reduction strength of a specific molecular chromophore is to change the activity/concentration of the oxidized or reduced species.

The importance of charge-transfer kinetics and interface/contact selectivity

If band-edge energy positions (at flat band) do not matter much for semiconductor photoelectrochemistry, what does? Charge-transfer kinetics and interface charge-carrier selectivity are crucial. Consider a photoelectrode that has been fabricated to have a buried n$^+$p junction, such as Pt/n$^+$p-Si, and used as an efficient photocathode for photoelectrochemical H$_2$ production (Fig. 3)[4]. The n$^+$p junction is selective towards the collection of photoexcited electrons over holes because of the higher conductivity of electrons compared with holes in the n$^+$ region[41]. Pt makes an Ohmic, unselective contact with the n$^+$-Si surface (emitter) layer, but that is inconsequential to the system behaviour because the n$^+$-Si layer is very thin and absorbs little light; the photocurrent is dominated by electron–hole pairs that separate at the n$^+$p junction before reaching the Pt/n$^+$-Si junction. The n$^+$p junction here is functionally equivalent to the case of strong inversion. Such an interface can be contrasted with Pt/p-Si, which is not very selective towards electrons over holes because the relative lack of interfacial band bending leads to substantial surface hole concentrations and hole conductivity. In all these cases, the absolute band edges of the semiconductor are irrelevant to the ability of the photoelectrode to drive an efficient Faradaic reaction.

In a simple model including carrier generation and interfacial charge transfer, Roe et. al. derived the limits on $V_{oc} \le (E_{fn} - E_{fp})/q$ across a two-contact (photovoltaic or photochemical) device. The set of four
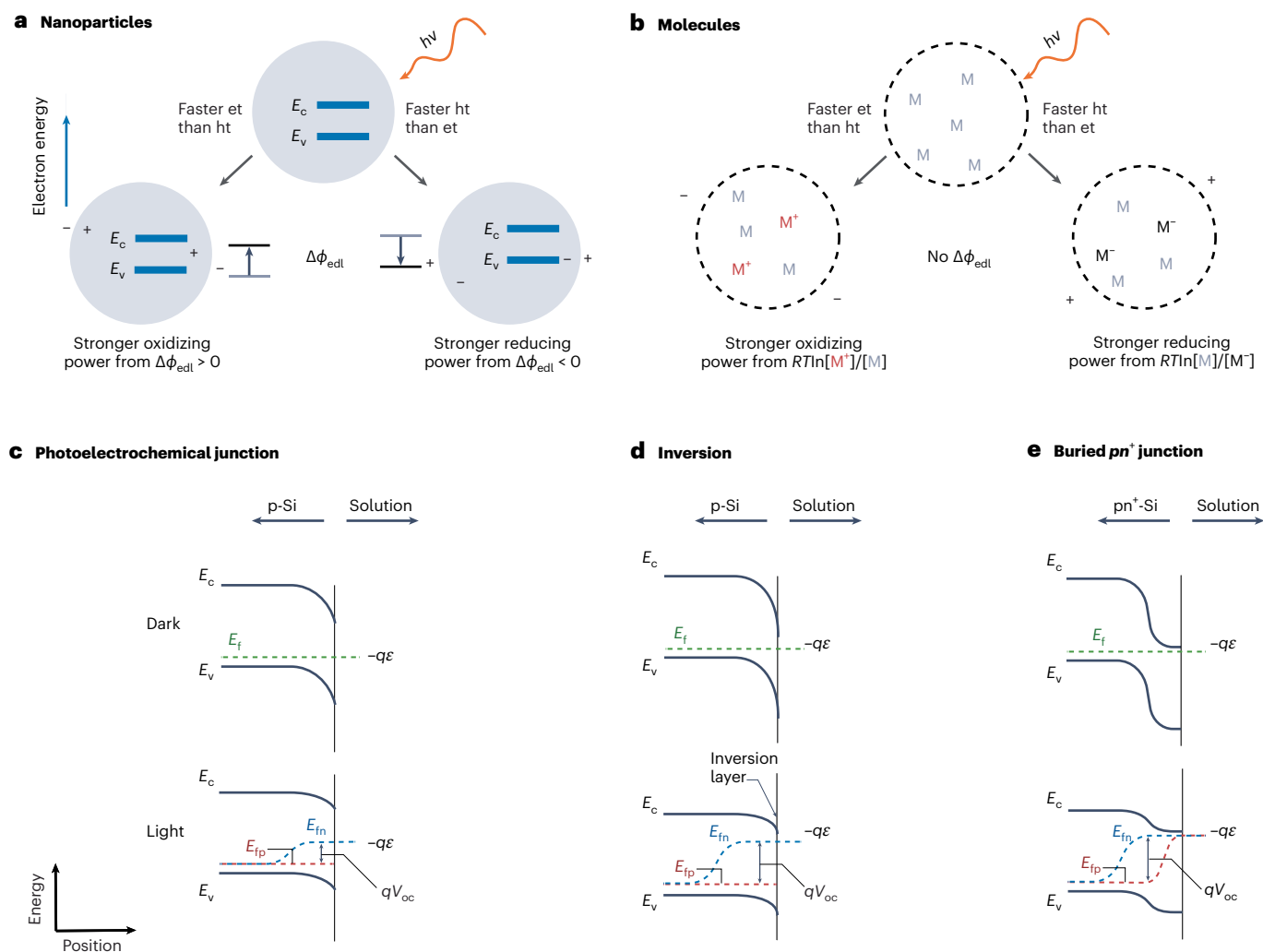
a **Nanoparticles**

Faster et than ht · Faster ht than et

E_c · E_v · hv

Stronger oxidizing power from $\Delta\phi_{edl} > 0$

$\Delta\phi_{edl}$

Stronger reducing power from $\Delta\phi_{edl} < 0$

b **Molecules**

Faster et than ht · Faster ht than et

No $\Delta\phi_{edl}$

Stronger oxidizing power from $RT\ln[M^+]/[M]$

Stronger reducing power from $RT\ln[M]/[M^-]$

c **Photoelectrochemical junction**

p-Si · Solution

Dark · E_c · E_f · $-q\varepsilon$ · E_v

Light · E_c · E_{fp} · E_{fn} · $-q\varepsilon$ · qV_{oc} · E_v

Energy / Position

d **Inversion**

p-Si · Solution

E_c · E_f · $-q\varepsilon$ · E_v

Inversion layer

E_c · E_{fp} · E_{fn} · $-q\varepsilon$ · qV_{oc} · E_v

e **Buried pn^+ junction**

pn^+-Si · Solution

E_c · E_f · $-q\varepsilon$ · E_v

E_c · E_{fp} · E_{fn} · $-q\varepsilon$ · qV_{oc} · E_v

Fig. 3 | Band diagrams and photochemical charge accumulation in nanoscopic and molecular systems. a, Due to the kinetic limitations of either electron transfer (et) or hole transfer (ht), nanoparticles can accumulate either multiple electrons or holes, respectively, at steady state. This process leads to changes in the reducing or oxidizing power of the carriers associated with changes in electrostatic potential profiles. **b**, Molecular energy levels are typically well spaced, leading to changes in the reducing or oxidizing power of

the ensemble via effects described by the Nernst equation and thus are more limited in range. **c**–**e**, Example band diagrams in the dark and under illumination for a photoelectrochemical junction in typical depletion conditions (**c**), with an inversion layer (**d**) and with a buried pn^+ junction (**e**). Note that both the inversion layer and the buried junction can equivalently shift E_c and E_v relative to the solution redox potential, as in this example, due to an additional electric potential drop across the electrical double layer.

rate equations for electron and hole partial currents, $J_n(x)$ and $J_p(x)$, at contacts x_1 and x_2 are given in Fig. 1 (ref. 42). The out-of-equilibrium surface electron and hole densities, $\Delta n = (n_x - n_x^{eq})$ and $\Delta p = (p_x - p_x^{eq})$, under illumination drive electron and hole partial currents. The magnitude of the current response is related directly to the kinetics of electron or hole transfer ($k_{1,et}$ or $k_{1,ht}$) and local species concentrations or, similarly, the equilibrium-exchange-current densities (J_{0n}^x and J_{0p}^x). The terms J_{0n}^x and J_{0p}^x define $(E_{fn} - E_{fp})/q$ and V_{oc} under steady-state illumination, and therefore the maximum free energy available to do work. Interfacial kinetics places limits on the maximum uphill chemical reaction that a photoabsorber can drive. This kinetic model applies identically to photoabsorbers beyond bulk semiconductors, including particulate photocatalysts, and could be adapted to molecular absorbers.

In particulate semiconductor photoelectrochemistry, the above considerations simultaneously apply to two spatially separated contacts on the same light-absorbing particle, with one contact selectively collecting electrons and the other holes[43–45]. The carrier selectivity of these contacts, along with the inherent properties of the semiconductor (mobility, lifetime, absorption coefficient), determine the ability

of the semiconductor to drive any given photochemical reaction with a specific ΔG_{rxn}. The measured absolute band-edge energies are of limited importance. Because many tests are carried out with sacrificial electron or hole acceptors (thus leading to the case where ΔG_{rxn} is near zero or even negative and spontaneous without light), understanding of the underlying physics has often been obscured. One example of such a system is the black (defective) TiO_2, which makes large amounts of H_2 under illumination only in the presence of fast sacrificial hole acceptors, despite the likely low absolute energy of the conduction band defect states and probable lack of photovoltage generation[46].

Corrosion and band edge energies

Gerischer proposed that semiconductors are inherently unstable in photoelectrochemical systems when the standard potentials for corrosion/decomposition are situated within the band edges[47]. For example, the anodic reaction $CdS + 2h^+ \rightarrow Cd^{2+} + S$ has a standard potential more negative on an electrochemical scale than the valence band of CdS. As a result, n-CdS is thermodynamically unstable in water under illumination. However, this does not mean that n-CdS and other semiconductors with similar energetics cannot function meaningfully as

photoelectrodes in water. The prolonged and stabilized operation of n-type CdS, ZnO, Cu_2O, CdTe and metal dichalcogenide photoanodes in water has been achieved through the manipulation of interfacial kinetics in two ways. One strategy is to alter the electrolyte chemistry so that the redox reactions of interest greatly outpace the undesirable corrosion reactions for the flux of photogenerated carriers. Kinetic strategies that speed up the rate of productive reactions for electrons and holes through electrocatalysis will lower the steady-state population of electrons and holes at the surface (and quasi-Fermi-level splitting), also suppressing the competing corrosion reactions[48]. A second strategy is to coat the semiconductor surface with a protective thin film that specifically impedes corrosion/decomposition processes[49–51]. Such protective surface layers generally form a buried-junction-type structure where the charge-carrier selectivity of the passivating surface layer in contact with the bulk semiconductor controls the ability of the semiconductor to drive a specific reaction. We also note that because corrosion reactions take place on the semiconductor surface, and thus inside the electrical double layer, their relative potentials shift in the same way as the band-edge potential if the semiconductor moves into inversion or accumulation, that is, corrosion reactions are not outer-sphere processes.

Conclusion

We have clarified a common misconception of band-edge alignment with reduction potentials as a key material design principle for photocatalysts. Semiconductor absorbers can support excess charge densities where the kinetics of surface reactions will determine the resulting products. This clarification enables research of perhaps previously ignored materials and informs design principles for photocatalyst systems engineering for both one-electron redox reactions and more-complex multi-electron-transfer reactions (for example, H_2 evolution, H_2O oxidation and CO_2 reduction). In multi-electron-transfer reactions, charge often accumulates at surface sites and how that charge is screened by electrolyte ions determines whether or not the apparent band edges shift with charge accumulation[15]. In the search for earth-abundant and efficient photocatalysts, the two primary materials properties of importance are sufficient optoelectronic properties of the absorber (optical absorption coefficient and free-carrier lifetime) and the ability to make both hole- and electron-carrier-selective contacts that connect the semiconductor with the catalytic sites that drive the oxidation and reduction half reactions of interest.

References

1. Li, J. & Wu, N. Semiconductor-based photocatalysts and photoelectrochemical cells for solar fuel generation: a review. *Catal. Sci. Technol.* **5**, 1360–1384 (2015).
2. Chen, S., Takata, T. & Domen, K. Particulate photocatalysts for overall water splitting. *Nat. Rev. Mater.* **2**, 17050 (2017).
3. Nozik, A. J. Photoelectrochemistry: applications to solar energy conversion. *Annu. Rev. Phys. Chem.* **29**, 189–222 (1978).
4. Boettcher, S. W. et al. Photoelectrochemical hydrogen evolution using Si microwire arrays. *J. Am. Chem. Soc.* **133**, 1216–1219 (2011).
5. Weber, M. F. & Dignam, M. J. Efficiency of splitting water with semiconducting photoelectrodes. *J. Electrochem. Soc.* **131**, 1258–1265 (1984).
6. Marcus, R. A. Chemical and electrochemical electron-transfer theory. *Annu. Rev. Phys. Chem.* **15**, 155–196 (1964).
7. Marcus, R. A. & Sutin, N. Electron transfers in chemistry and biology. *Biochim. Biophys. Acta Rev. Bioenerg.* **811**, 265–322 (1985).
8. Fajardo, A. M. & Lewis, N. S. Rate constants for charge transfer across semiconductor-liquid interfaces. *Science* **274**, 969–972 (1996).
9. Lewis, N. S. Chemical control of charge transfer and recombination at semiconductor photoelectrode surfaces. *Inorg. Chem.* **44**, 6900–6911 (2005).
10. Memming, R. in *Semiconductor Electrochemistry* 127–168 (Wiley-VCH, 2015).
11. Moore, C. C. Ergodic theorem, ergodic theory, and statistical mechanics. *Proc. Natl Acad. Sci. USA* **112**, 1907–1911 (2015).
12. Hisatomi, T., Kubota, J. & Domen, K. Recent advances in semiconductors for photocatalytic and photoelectrochemical water splitting. *Chem. Soc. Rev.* **43**, 7520–7535 (2014).
13. Ager, J. W., Shaner, M. R., Walczak, K. A., Sharp, I. D. & Ardo, S. Experimental demonstrations of spontaneous, solar-driven photoelectrochemical water splitting. *Energy Environ. Sci.* **8**, 2811–2824 (2015).
14. Chen, Z. et al. Accelerating materials development for photoelectrochemical hydrogen production: standards for methods, definitions, and reporting protocols. *J. Mater. Res.* **25**, 3–16 (2010).
15. Laskowski, F. A. L., Nellist, M. R., Qiu, J. & Boettcher, S. W. Metal oxide/(oxy)hydroxide overlayers as hole collectors and oxygen-evolution catalysts on water-splitting photoanodes. *J. Am. Chem. Soc.* **141**, 1394–1405 (2019).
16. Lyon, L. A. & Hupp, J. T. Energetics of the nanocrystalline titanium dioxide/aqueous solution Interface: approximate conduction band edge variations between $H_0 = -10$ and $H_- = +26$. *J. Phys. Chem. B* **103**, 4623–4628 (1999).
17. Lichterman, M. F. et al. Direct observation of the energetics at a semiconductor/liquid junction by operando X-ray photoelectron spectroscopy. *Energy Environ. Sci.* **8**, 2409–2416 (2015).
18. Peper, J. L., Gentry, N. E., Boudy, B. & Mayer, J. M. Aqueous TiO_2 nanoparticles react by proton-coupled electron transfer. *Inorg. Chem.* **61**, 767–777 (2022).
19. Kautek, W. & Gerischer, H. Photoelectrochemical reactions and formation of inversion layers at n-type MoS_2, $MoSe_2$, and WSe_2 electrodes in aprotic solvents. *Ber. Bunsen Ges. Phys. Chem.* **84**, 645–653 (1980).
20. Jaeger, C. D., Gerischer, H. & Kautek, W. Formation of an inversion layer in n-type $MoSe_2$ electrodes: observation in the presence of highly oxidizing redox systems. *Ber. Bunsen Ges. Phys. Chem.* **86**, 20–25 (1982).
21. Royea, W. J., Michalak, D. J. & Lewis, N. S. Role of inversion layer formation in producing low effective surface recombination velocities at Si/liquid contacts. *Appl. Phys. Lett.* **77**, 2566–2568 (2000).
22. Grimm, R. L. et al. Comparison of the photoelectrochemical behavior of H-terminated and methyl-terminated Si(111) surfaces in contact with a series of one-electron, outer-sphere redox couples in CH_3CN. *J. Phys. Chem. C* **116**, 23569–23576 (2012).
23. Gstrein, F., Michalak, D. J., Knapp, D. W. & Lewis, N. S. Near-surface channel impedance measurements, open-circuit impedance spectra, and differential capacitance vs potential measurements of the Fermi level position at Si/CH_3CN contacts. *J. Phys. Chem. C* **111**, 8120–8127 (2007).
24. Park, K.-W. & Kolpak, A. M. Optimal methodology for explicit solvation prediction of band edges of transition metal oxide photocatalysts. *Commun. Chem.* **2**, 79 (2019).
25. Trasatti, S. The absolute electrode potential: an explanatory note. *Pure Appl. Chem.* **58**, 955–966 (1986).
26. Sze, S. M. & Ng, K. K. *Physics of Semiconductor Devices* (John Wiley, 2006).
27. Michalak, D. J. & Lewis, N. S. Use of near-surface channel conductance and differential capacitance versus potential measurements to correlate inversion layer formation with low effective surface recombination velocities at *n*-Si/liquid contacts. *Appl. Phys. Lett.* **80**, 4458–4460 (2002).
28. Turner, J. A., Manassen, J. & Nozik, A. J. Photoelectrochemistry with *p*-Si electrodes: effects of inversion. *Appl. Phys. Lett.* **37**, 488–491 (1980).

29. Keller, N. D. et al. Multi-electron transfer at H-terminated p-Si electrolyte interfaces: large photovoltages under inversion conditions. *J. Am. Chem. Soc.* **145**, 11282–11292 (2023).

30. Bard, A. J., Bocarsly, A. B., Fan, F. R. F., Walton, E. G. & Wrighton, M. S. The concept of Fermi level pinning at semiconductor/liquid junctions. Consequences for energy conversion efficiency and selection of useful solution redox couples in solar devices. *J. Am. Chem. Soc.* **102**, 3671–3677 (1980).

31. Bocarsly, A. B., Bookbinder, D. C., Dominey, R. N., Lewis, N. S. & Wrighton, M. S. Photoreduction at illuminated p-type semiconducting silicon photoelectrodes. Evidence for Fermi level pinning. *J. Am. Chem. Soc.* **102**, 3683–3688 (1980).

32. Spitler, M. T. Impedance analysis of semiconductor electrodes in the accumulation region. *Sustain. Energy Fuels* **7**, 5301–5309 (2023).

33. Hofstein, S. R. & Warfield, G. Physical limitations on the frequency response of a semiconductor surface inversion layer. *Solid-State Electron.* **8**, 321–341 (1965).

34. Madou, M. J., Loo, B. H., Frese, K. W. & Morrison, S. R. Bulk and surface characterization of the silicon electrode. *Surf. Sci.* **108**, 135–152 (1981).

35. Cooper, G., Turner, J. A. & Nozik, A. J. Mott–Schottky plots and flatband potentials for single crystal rutile electrodes. *J. Electrochem. Soc.* **129**, 1973–1977 (1982).

36. Thapar, R. & Rajeshwar, K. Mott–Schottky analyses on n- and p-GaAs/room temperature chloroaluminate molten-salt interfaces. *Electrochim. Acta* **28**, 195–198 (1983).

37. Bardwell, J. A., Draper, N. & Schmuki, P. Growth and characterization of anodic oxides on Si(100) formed in 0.1 M hydrochloric acid. *J. Appl. Phys.* **79**, 8761–8769 (1996).

38. Huygens, I. M. & Strubbe, K. Electrochemical impedance study of the germanium/electrolyte interface. *J. Electrochem. Soc.* **155**, F49 (2008).

39. La Mantia, F., Habazaki, H., Santamaria, M. & Di Quarto, F. A critical assessment of the Mott–Schottky analysis for the characterisation of passive film–electrolyte junctions. *Russ. J. Electrochem.* **46**, 1306–1322 (2010).

40. Molto, C., Etcheberry, A., Grand, P. P. & Goncalves, A. M. Study of photo-oxidized n-type textured silicon surface through electrochemical impedance spectroscopy. *J. Electrochem. Soc.* **167**, 146505 (2020).

41. Würfel, P. & Würfel, U. *Physics of Solar Cells: From Basic Principles to Advanced Concepts* 3rd edn (Wiley-VCH, 2016).

42. Roe, E. T., Egelhofer, K. E. & Lonergan, M. C. Limits of contact selectivity/recombination on the open-circuit voltage of a photovoltaic. *ACS Appl. Energy Mater.* **1**, 1037–1046 (2018).

43. Pan, Z. et al. Elucidating charge separation in particulate photocatalysts using nearly intrinsic semiconductors with small asymmetric band bending. *Sustain. Energy Fuels* **3**, 850–864 (2019).

44. Pan, Z. et al. Mutually-dependent kinetics and energetics of photocatalyst/co-catalyst/two-redox liquid junctions. *Energy Environ. Sci.* **13**, 162–173 (2020).

45. Liu, T. et al. A general interfacial-energetics-tuning strategy for enhanced artificial photosynthesis. *Nat. Commun.* **13**, 7783 (2022).

46. Chen, X., Liu, L., Yu, P. Y. & Mao, S. S. Increasing solar absorption for photocatalysis with black hydrogenated titanium dioxide nanocrystals. *Science* **331**, 746–750 (2011).

47. Gerischer, H. On the stability of semiconductor electrodes against photodecomposition. *J. Electroanal. Chem. Interfac. Electrochem.* **82**, 133–143 (1977).

48. Yu, W. Understanding the stability of semiconducting photocathodes for solar water splitting. *Curr. Opin. Electrochem.* **39**, 101262 (2023).

49. Zhao, T. et al. A coating strategy to achieve effective local charge separation for photocatalytic coevolution. *Proc. Natl Acad. Sci. USA* **118**, e2023552118 (2021).

50. Shen, X. et al. Tuning intermediate bands of protective coatings to reach the bulk-recombination limit of stable water-oxidation GaP photoanodes. *Adv. Energy Mater.* **12**, 2201314 (2022).

51. Shen, X. et al. Comprehensive evaluation for protective coatings: optical, electrical, photoelectrochemical, and spectroscopic characterizations. *Front. Energy Res.* **9**, 799776 (2022).

Acknowledgements

Author contributions

A.J.K. and S.W.B. initiated the Perspective. A.J.K. wrote the first draft and generated its figures. A.C.N., G.J.M., S.M. and S.A. edited and contributed substantially to articulating the concepts. A.J.K. and S.W.B. wrote the final paper with input from all authors.

Competing interests

The authors declare no competing interests.

Additional information

Correspondence should be addressed to Shannon W. Boettcher.

Peer review information *Nature Catalysis* thanks the anonymous reviewers for their contribution to the peer review of this work.

Reprints and permissions information is available at www.nature.com/reprints.